DE GRUYTER

Chemical Papers
DOI: 10.1515/chempap-2015-0192

ORIGINAL PAPER

A novel triphenylamine-based dye sensitizer supported on titania nanoparticles and the effect of titania fabrication on its optical properties

[a]Elisa Moretti*, [a]Manuela Aversa, [a] Alberto Scrivanti, [a]Loretta Storaro, [a]Aldo Talon, [a]Riccardo Marin, [b]Juan Antonio Cecilia, [b]Enrique Rodríguez-Castellón, [a,c]Stefano Polizzi

[a]*Department of Molecular Sciences and Nanosystems,* [c]*Electron Microscopy Center "Giovanni Stevanato", Universitá Ca' Foscari Venezia, Via Torino 155/B, 30172 Venezia, Italy*

[b]*Department of Inorganic Chemistry, Crystallography and Mineralogy, Faculty of Sciences, Universidad de Málaga, Campus de Teatinos, E-29071 Málaga, Spain*

Received 24 March 2015; Revised 30 June 2015; Accepted 30 June 2015

A new synthesised triphenylamine-based dye having a branched structure with one OH-ending branch able to interact with the surface hydroxyl moieties of mesoporous TiO_2 is reported. Optical properties of the dye-titania hybrid material are presented and the higher efficiency of the dye on pure anatase TiO_2 compared to the commercial Degussa P25, which contains a rutile phase component, is confirmed. The optical and chemical properties of the dye make it a promising candidate as a metal-free dye for DSSCs or as a host for a variety of transition or main group metal ions for different applications.

Keywords: triarylamine dye sensitizer, titania, anatase, hybrid materials

Introduction

In recent years, many functional materials have been obtained from covalent grafting of organic dyes on inorganic surfaces for analytical applications (Pesek, 1990; Gómez-Romero & Sanchez, 2004), the development of optical devices, and functionalisation of nanoparticles for medical diagnosis (Ganschow et al., 2000; Zhao et al., 2005), since an organized inorganic framework usually prevents dye molecules aggregation. On the other hand, the preparation of hybrid systems by covalent grafting on an inorganic network offers materials where the host imposes a specific and organized orientation to the guest active molecules (Gómez-Romero & Sanchez, 2004). Among the numerous possible inorganic acceptors, layered inorganic matrices, as clays and hydrotalicites, or metal oxides, as silica and titania, have been investigated (Moretti et al., 2012; Latterini et al., 2007; de Jesus Trindade et al., 2011; Segal-Peretz et al., 2014). In particular, TiO_2 can be considered a promising host material due to its low toxicity, good electron conductivity, and electron-accepting character with respect to other oxidic materials.

Over the past years, dye organic sensitizers based on triarylamine have been widely investigated as components of electro-optical functional materials due to their good electro-donating ability, hole-transport properties and non-planarity of the triarylamine unit that prevents aggregation. For instance, some triarylamine dyes have been employed as sensitizers in dye-sensitized solar cells (DSSCs) giving overall DSSC efficiencies very close to that achievable by the Grätzel N3 dye (Gu et al., 2012; Hagberg et al., 2008; Zhang et al., 2009a).

While the first examples of photosensitizers devel-

*Corresponding author, e-mail: elisa.moretti@unive.it

oped by Grätzel were based on ruthenium complexes (Grätzel, 2009) on TiO_2, and some authors (Urankar et al., 2010; Amadio et al., 2011) studied two chelating pyridyl groups to host a variety of metal ions; over the past two decades, considerable efforts have been done to find metal-free organic sensitizers (Sharifi et al., 2014).

By now, the best performing metal-free dyes show efficiencies not far from those of the best Ru-dyes and offer additional advantages, such as simpler synthetic procedures, lower manufacturing costs, and the possibility of uncomplicated tuning of their optical characteristics (Hagfeldt et al., 2010).

While considerable synthetic effort has been done in order to introduce a great variety of light adsorbing moieties in sensitizer structures, no special attention has been paid to structural variations of the anchoring group that should assure adhesion of the dye on the TiO_2 surface and allow charge injection. In fact, not so many alternatives to the carboxylic acid moiety have been employed as anchoring groups up to now (Ardo & Meyer, 2009; Nazeeruddin et al., 2004; Wang et al., 2000; Ooyama et al., 2011; Harima et al., 2013; Katono et al., 2011; Mao et al., 2012; Michinobu et al., 2014).

As a part of a research program devoted to the development of organic sensitizers with extended dendritic structures, a branched wedge based on triphenylamine was prepared. Some of the key features of this dye sensitizer are the presence of a triarylamine moiety, extended π systems of the triazole rings, and a benzyl alcohol functionality at the focal point.

In the synthesis of the chromophore, a major role is played by the copper-catalyzed azide-alkyne [3+2] cycloaddition which allows a very efficient insertion of the triazole rings into the structure (Bolje et al., 2014). This reaction has gained an outstanding importance among the synthetic tools employed in the preparation of optoelectronic materials as it tolerates the presence of a wide variety of functional groups (Duan et al., 2012; Li et al., 2010; Parent et al., 2005). Moreover, it proceeds under very mild conditions with high selectivity and high overall yields so that it meets the Sharpless's requirements to be defined as a "click" reaction (Rostovtsev et al., 2002; Kolb et al., 2001).

In this paper, the synthesis of a branched wedge based on triphenylamine and a preliminary study of its potential use as a sensitizer supported on TiO_2 nanoparticles are presented. By comparing the results obtained by employing two different titania matrices, it seems that the TiO_2 fabrication method has an important role in the determination of the optical properties of the DS-TiO_2 hybrid material.

Experimental

Materials and methods

All organic syntheses were carried out under nitrogen atmosphere in Schlenk-type glassware.

All reagents were purchased from Aldrich (Milan, Italy) and used as received. Commercial solvents (Aldrich) were purified as described in literature (Armarego & Perrin, 1996). 2-(Azidomethyl)pyridine was prepared according to a literature procedure (Brotherton et al., 2009). Commercially available titanium dioxide, P25 (Degussa-Huls (Parsippany, NJ, USA), 70 % anatase, 30 % rutile), with a BET surface area of 55 $m^2\ g^{-1}$ and a nominal average particle size of 30 nm, was used for comparison with a freshly synthesised anatase pure phase titania (see Paragraph "Synthesis of mesoporous anatase titania nanoparticles".)

Elemental chemical analyses (C, H, N, S) were performed on a LECO CHNS-932 analyzer (Madrid, Spain).

^1H and ^{13}C NMR spectra were recorded on a Bruker AVANCE 300 spectrometer (Milan, Italy) operating at 300.1 MHz and 75.4 MHz, respectively. The chemical shift values are reported in δ units with reference to the residual solvent signal. The ^{13}C chemical shift values were assigned through DEPT-135 and 2D-heteronuclear correlation experiments (HMQC and HMBC).

X-ray powder diffraction (XRPD) patterns were obtained using a Philips X'Pert system (Eindhoven, The Netherlands). Data were recorded with the step size of 0.05°, in the 10–80° 2θ range. Intensities were collected in a pre-set time mode (10 s). A system equipped with a focusing graphite monochromator on the diffracted beam and with a proportional counter with an electronic pulse height discriminator was used. Moreover, a divergence slit of 0.5°, a receiving slit of 0.2 mm, an anti-scatter slit of 0.5°, and Ni filtered CuK_α radiation (20 mA, 40 kV) were employed. Samples were disc shaped pressed powders and the spectra were collected after their calcination. The average sizes of the crystallites were obtained by the Fourier method applied to the analytical diffraction peak profiles, which are constrained couples of pseudo-Voigt functions (describing the $K_{\alpha1}$–$K_{\alpha2}$ doublets) as described elsewhere (Enzo et al., 1985, 1988). The volume-weighted average crystalline sizes $<D>_{hkl}$, measured perpendicularly to the (hkl) lattice planes, were determined in correspondence with the most intense (101) peak profiles of the TiO_2 anatase phase. The Fourier transforms of the measured peak profiles were corrected for instrumental broadening using the very narrow lines of a reference standard sample (α-quartz). The peak broadening was attributed to the crystallite size effect only. The estimated errors on the crystalline sizes obtained by this procedure were about 10 %.

Field Emission Gun-Scanning Electron Microscopy (FEG-SEM) images were taken on a Zeiss SIGMA VP (Überkochen, Germany) using the in-lens secondary electron (Everhart–Thornley) detector.

A JEOL JEM 3010 microscope (Tokyo, Japan) operating at 300 kV with a high resolution pole-piece (0.17 nm point-to-point resolution) and equipped with a Gatan Multiscan CCD camera model 794 (Pleasanton, CA, USA) was used for transmission electron microscopy (TEM). Samples both for SEM and for TEM analyses were prepared by evaporation of one drop of a suspension of the TiO_2 powder in isopropyl alcohol obtained by sonication on a copper grid coated with an amorphous carbon holey film.

Nitrogen adsorption–desorption measurements were performed at the liquid nitrogen temperature of (–196 ℃) by a Micromeritics ASAP 2010 apparatus (Peschiera Borromeo, Italy). Before each measurement, the samples (0.1 g) were outgassed first at 130 ℃ for 12 h at 0.67 Pa and then at room temperature for 2 h at 1×10^{-4} Pa. The N_2 isotherms were used to determine the specific surface areas through the BET equation (S_{BET}), and the specific pore volume (V_{p}) calculated at $P/P^{\circ} = 0.98$.

Infrared spectra in the diffuse reflectance mode (DRIFT-IR) were acquired between 4000 cm^{-1} and 400 cm^{-1} on a FT-IR NICOLET Magna-IR^{TM} instrument by Thermo Fisher Scientific (Rodano, Italy), with an AVATAR 360 FT-IR E.S.P accessory. The resolution was kept at 4 cm^{-1} and the spectra were measured using the KBr technique (5 mass % of sample in KBr).

X-Ray photoelectron spectra (XPS) were collected using a Physical Electronics PHI 5700 spectrometer (Madrid, Spain) with non-monochromatic MgK_{α} radiation (300 W, 15 kV, 1253.6 eV) for the analysis of the core level signals of C 1s, O 1s, N 1s, Cu 2p, and Ti 2p and with a multi-channel detector. Spectra of the powdered samples were recorded at the constant pass energy values of 29.35 eV, using a 720 μm diameter analysis area. During data processing of the XPS spectra, binding energy values were referenced to the C 1s peak (284.8 eV) from the adventitious contamination layer.

The PHI ACCESS ESCA-V6.0 F software package was used for data acquisition and analysis. A Shirley-type background was subtracted from the signals. Recorded spectra were always fitted using the Gauss–Lorentz curves in order to determine the binding energy of the different element core levels more accurately. The error in BE was estimated to be of ca. 0.1 eV.

Photoluminescence excitation (PLE) and emission (PL) measurements were carried out using a Jobin Yvon Fluorolog-3 spectrofluorimeter by HORIBA Jobin Yvon (Milan, Italy). A xenon arc lamp was used as the continuous-spectrum source selecting the excitation wavelength by a double Czerny–Turner monochromator, while the detection system was constituted by a single grating monochromator coupled to a PMT for measurements in the visible spectra range.

Preparation of dye sensitizer (DS), mesoporous anatase titania nanoparticles, and DS-titania hybrid material

Synthesis of 4-(diphenylamino)benzaldehyde (**2**) was adapted from Park et al. (2000) with slight modifications. Dry *N*,*N*-dimethylformamide (DMF) (6.0 mL, 77.6 mmol) was, under nitrogen atmosphere, added to a 100 mL two-necked flask equipped with a nitrogen inlet, a magnetic stirrer and a condenser. After cooling the reaction flask to 0 ℃, 2.0 mL of phosphorus oxychloride (3.13 g, 20.4 mmol) were added dropwise under stirring. The mixture was allowed to reach room temperature then triphenylamine (TPA, **1)** (5.0 g, 20.4 mmol) and dry DMF (15.0 mL) were added. The mixture was heated at 80 ℃ for 6 h under stirring, cooled and poured into chilly water containing 6.0 g of sodium acetate under vigorous stirring. The precipitated yellow solid was washed with water and purified by flash chromatography (silica gel/toluene). The desired product was obtained as a yellow powder (4.87 g, 17.8 mmol, 87 % yield) and its ^{1}H NMR spectrum was found in accordance with literature data (Park et al., 2000).

4-(Bis(4-iodophenyl)amino)benzaldehyde (**3**) was synthesized by contacting 4-(diphenylamino)benzaldehyde **(2)** (3.8 g, 13.9 mmol), potassium iodide (3.0 g, 18.1 mmol), acetic acid (45.0 mL) and deionized water (5.0 mL) in a 100 mL two-neck flask equipped with a nitrogen inlet, a magnetic stirrer, and a condenser. After heating the reaction mixture to 80 ℃, potassium iodate (2.98 g, 13.9 mmol) was added in one portion and the resulting mixture was kept at 80 ℃ under stirring for 5 h. The solution was allowed to cool to room temperature and it was poured into ice-water under stirring. Yellow precipitate was collected by filtration and treated with a 5 mass % $NaHSO_3$ solution (40.0 mL). Upon filtration, the desired aldehyde was obtained as a yellow solid (**3**) (7.0 g, 13.4 mmol, 96 % yield), the ^{1}H NMR spectrum of which was found in accordance with literature data (Ning et al., 2007).

(4-(Bis(4-iodophenyl)amino)phenyl)methanol (**4**) was obtained in a round-bottom flask containing 4-(bis(4-iodophenyl)amino)benzaldehyde (**3**) (3.94 g, 7.51 mmol) in EtOH (34.0 mL) and CH_2Cl_2 (34.0 mL). $NaBH_4$ (297.0 mg, 7.82 mmol) was slowly added and the reaction mixture was kept under stirring at room temperature for 3 h.

The resulting mixture was poured into deionized water (70.0 mL) and extracted with ethyl acetate; the recovered organic phase was washed with water, dried over $MgSO_4$ and taken to dryness under reduced pressure. The obtained solid was purified by column chromatography (silica gel/dichloromethane) to give **4** as a white solid (3.93 g, 7.45 mmol, 98 % yield).

(4-(Bis(4-((trimethylsilyl)ethynyl)phenyl)amino) phenyl)methanol (**5**) was prepared as follows: (4-(bis(4-iodophenyl)amino)phenyl)methanol (**4**) (396.0

mg, 0.751 mmol), toluene (13.0 mL), and trimethylsilylacetylene (176.4 mg, 1.8 mmol) were added to a flame-dried two-neck flask equipped with a nitrogen inlet, a magnetic stirrer, and a condenser. After three successive vacuum/nitrogen cycles, diisopropylamine (4.0 mL), $Pd(PPh_3)_4$ (11.1 mg, 0.00961 mmol) and CuI (2.2 mg, 0.0116 mmol) were introduced and the mixture was stirred under nitrogen at 80 °C overnight. The reaction mixture was cooled and extracted with CH_2Cl_2 at room temperature. The organic phase was washed with water and brine, dried over $MgSO_4$ and rotoevaporated. The crude reaction product was purified by flash-chromatography (silica gel, eluent: pentane/$CH_2Cl_2 = 1 : 1$) to give **5** (309 mg, 0.662 mmol, 88 % yield) of the title compound as a yellow powder.

Synthesis of (4-(bis(4-ethynylphenyl)amino)phenyl) methanol (**6**) was carried out as follows: a mixture of (4-(bis(4-((trimethylsilyl)ethynyl)phenyl)amino) phenyl)methanol (**5**) (309 mg, 0.662 mmol), K_2CO_3 (927 mg, 6.72 mmol), tetrahydrofuran THF (13 mL), and methanol (13 mL) was stirred at room temperature for 90 min. Then, the reaction mixture was diluted with water and extracted with CH_2Cl_2. The organic layer was dried over $MgSO_4$, filtered and taken to dryness. The crude product was purified by flash-chromatography (silica gel, eluent: CH_2Cl_2/ethyl acetate, 9.5 : 0.5) to give the title compound (**6**) (210 mg, 0.648 mmol, 98 % yield) as a yellow powder.

Finally, (4-(bis(4-(1-(pyridin-2-ylmethyl)-1H-1,2, 3-triazol-4-yl)phenyl)amino)phenyl)methanol (**7**) was obtained. A mixture of (4-(bis(4-ethynylphenyl)amino) phenyl)methanol (**6**) (209.5 mg, 0.648 mmol) and 2-(azidomethyl)pyridine (183 mg, 1.36 mmol) in THF/H_2O (4 : 1, 15 mL) was stirred at room temperature overnight in the presence of 10 mole % of $CuSO_4 \cdot 5H_2O$ and 20 mole % of sodium ascorbate. The reaction mixture was partially concentrated under reduced pressure and extracted with CH_2Cl_2 (3×20 mL). The combined organic phases were dried with $MgSO_4$ and concentrated. Dilution with diethyl ether of the concentrated methylene chloride solution led to the precipitation of the dye sensitizer (DS) (**7**) as a pale yellow solid (371.5 mg, 0.628 mmol, 97 % yield).

Mesoporous anatase titania nanoparticles were synthesized according to the procedure reported by Chen et al. (2009) with slight modifications. Hexadecylamine (2.64 g, 10.95 mmol) was dissolved in ethanol (400 mL), followed by the addition of a 0.1 M KCl aqueous solution (1.60 mL). Titanium(IV) isopropoxide (8.8 mL, 29.7 mmol) was added under vigorous stirring at room temperature. The resulting TiO_2 suspension was kept static at the same temperature for 16 h and then the solid was collected by centrifugation, washed with ethanol, and dried in air at room temperature. In order to obtain a highly crystalline TiO_2 framework, the solvothermal process was used. Amorphous titania (3.0 g) was dispersed into a mixture of ethanol (38 mL) and deionized water (19 mL) and then, a 280 g L^{-1} aqueous ammonia solution (1.9 mL) was slowly added dropwise. The mixture was kept in a teflon autoclave at 160 °C under autogenous pressure for 16 h. The product was recovered by centrifugation, washed with ethanol, dried at room temperature, and finally calcined at 550 °C for 2 h. This sample was labeled as anatase in the following text.

Freshly synthesized mesoporous TiO_2 (1.00 g) was added to a yellow chloroform solution of the dye sensitizer (10.2 mg in 20 mL). Then, the resulting suspension was heated to reflux under nitrogen overnight, during which time, the organic phase became colorless. After removing the solvent under vacuum, a yellow solid was obtained (thereafter DS-Anatase), which was dried to constant mass at 50 °C and then ground in a mortar for spectroscopic and analytical investigations.

For comparison purposes, an additional sample was prepared using the commercial titania Degussa P25 as the inorganic matrix with the same loading (nominal 1.0 mass % of DS) and method of impregnation. The resulting material (thereafter DS-P25), a grayish solid, was dried to constant mass at 50 °C and then ground in a mortar for spectroscopic and analytical investigations.

The dye sensitizer content was determined by elemental analysis and estimated as 0.93 mass % on the fresh synthesized TiO_2 and as 0.91 mass % on Degussa P25 titania.

Results and discussion

Synthesis of the novel triphenylamine (TPA)-based branched dye sensitizer (DS) was carried out according to the strategy depicted in Fig. 1.

In the first step, the Vilsmeier reaction was employed to formylate commercial triphenylamine (**1**) according to a literature procedure (Park et al., 2000). Treatment of the resulting aldehyde (**2**) with KI/KIO_3 in acetic acid afforded the corresponding diiododerivative (**3**) as described by Ning et al. (2007). Reduction with $NaBH_4$ led to the benzyl alcohol derivative (**4**). Sonogashira coupling of the latter with trimethylsilylacetylene followed by basic removal of the protecting groups gave the terminal dialkyne (**6**). Finally, coupling of the dialkyne with 2-(azidomethyl)pyridine in the presence of an in situ generated Cu(I) catalyst afforded the target sensitizer (**7**). The adopted synthetic strategy was proved to be quite efficient with the overall yield as high as 70 %. All the new intermediates and the final dye sensitizer are soluble in common organic solvents (dichloromethane, chloroform, tetrahydrofuran, DMSO) and were characterized by elemental analysis and ^1H and ^{13}C NMR spectroscopy; the relevant data are reported in Tables 1 and 2.

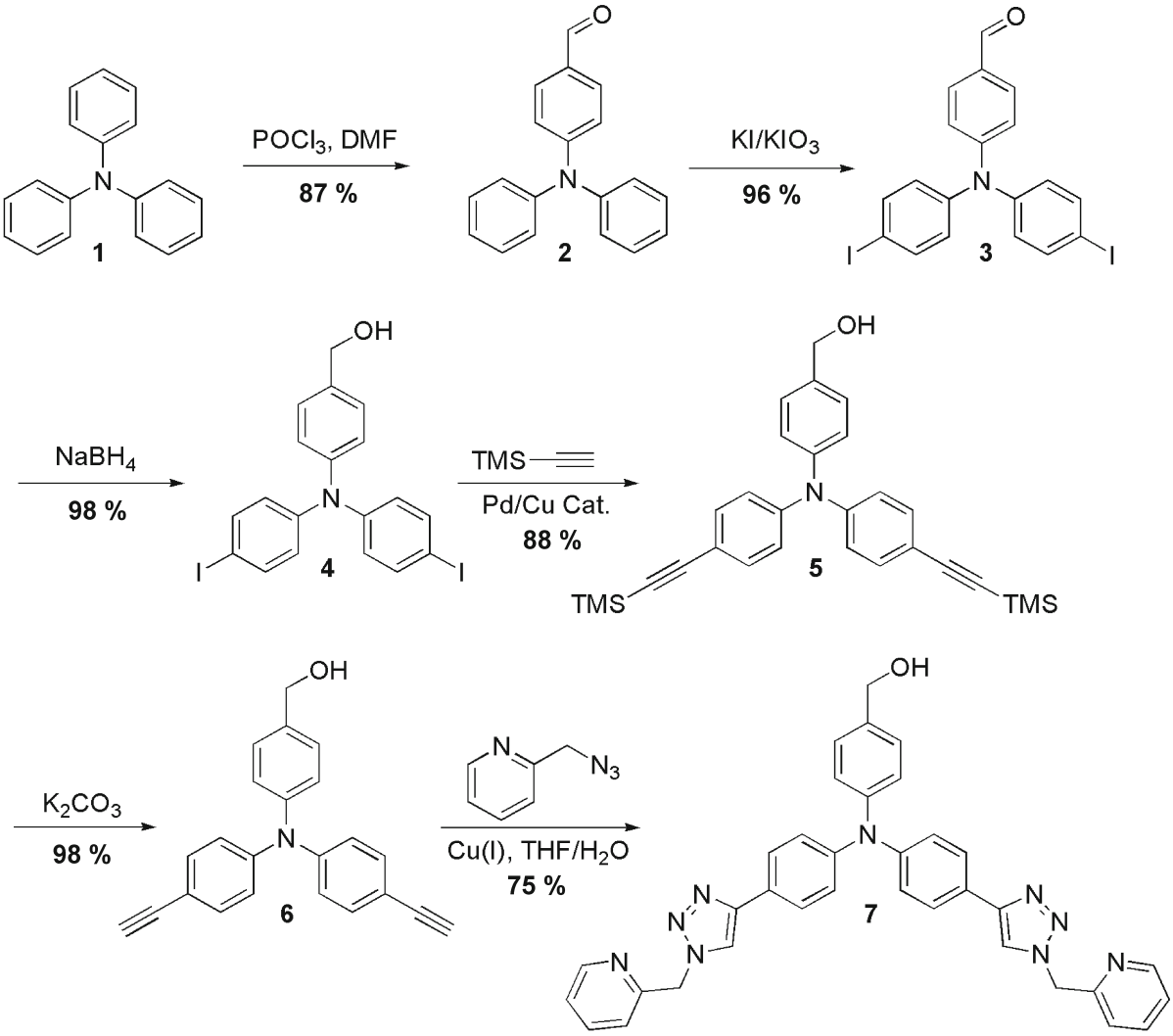

Fig. 1. Synthetic route for the synthesis of the triphenylamine-based dye sensitizer.

Very convenient impregnation of the supports was easily accomplished by simple stirring of a titania suspension in a diluted chloroform solution of the dye. ^{1}H NMR spectroscopy showed that the chromophore was completely adsorbed by the inorganic matrix. In fact, a small amount of final hybrid materials was suspended in $CDCl_3$ under heating to determine the possible leaching of DS and the signals of the free dye in $CDCl_3$ solution were totally absent in the aromatic range of the ^{1}H NMR spectrum.

Morphology of the titania samples was characterized by scanning and transmission electron microscopy (SEM and TEM). A typical large-scale FEG-SEM image of the prepared mesoporous anatase TiO_2 after the solvothermal process and calcination (Fig. 2a) displays a structure made of agglomerates of nanoparticles. TEM images give more detailed information about the single nanoparticles (Figs. 2b and 2c), and show that nanocrystals have different shapes with many faceted crystals, some with a rectangular shape, a few rice-like shaped ones, and some typical truncated bipyramids (Barnard & Curtis, 2005). The HRTEM image (Fig. 2c) also shows that some particles are not single-crystals and that most of the particles have a porous structure with pores of 2–3 nm in size. Most particles of the anatase sample are in the 20–30 nm size range, somewhat smaller than those of Degussa P25 (Fig. 2d).

An analysis of the fresh synthesized titania by N_2 adsorption–desorption at –196 °C, after the solvothermal and calcination treatment, exhibited a type IV isotherm (not shown) typical of a mesoporous material with the cumulative volume equal to 0.36 $cm^3\ g^{-1}$ and the BET specific surface area of 74 $m^2\ g^{-1}$, which is significantly higher than the values obtained for commercial Degussa P25 titania (0.06 $cm^3\ g^{-1}$ and 55 $m^2\ g^{-1}$, respectively), due to the smaller size of the particles and possibly to the pores (in case of open pores accessible to the gas).

Molecular coverage of the adsorbed dye sensitizer per unit surface area of the two titania samples was calculated by elemental analysis of the dye sensitizer-

Table 1. ^{1}H and ^{13}C NMR spectral data of the prepared compounds

Compound	Spectral data
2	^{1}H NMR (300 MHz, $CDCl_3$) δ: 9.79 (s, 1H, CHO), 6.97–7.75 (m, 14H)
3	^{1}H NMR (300 MHz, $CDCl_3$) δ: 9.84 (s, 1H, CHO), 7.73 (d, 2H, arom), 7.65 (d, 4H, arom), 7.07 (d, 2H, arom), 6.90 (d, 4H, arom)
4	^{1}H NMR (300 MHz, CD_2Cl_2) δ: 7.53 (d, 4H, arom), 7.30 (d, 2H, arom), 7.07 (d, 2H, arom), 6.83 (d, 4H, arom), 4.63 (s, 2H), 1.66 (br s, 1H, OH) ^{13}C NMR (75 MHz, $CDCl_3$) δ: 147.2, 146.4, 138.4, 136.5, 128.6, 125.9, 124.9, 88.1, 65.0
5	^{1}H NMR (300 MHz, CD_2Cl_2) δ: 7.34–7.29 (m, 6H, arom), 7.09–7.06 (m, 2H, arom), 6.98–6.95 (d, 4H, arom), 4.65–4.63 (d, 2H, OCH_2), 1.77 (t, 1H, OH), 0.23 (s, 18H, CH_3) ^{13}C NMR (75 MHz, CD_2Cl_2) δ: 147.9, 146.5, 138.1, 133.5, 128.7, 126.1, 123.7, 117.6, 105.8, 94.0, 64.7, 0.3
6	^{1}H NMR (300 MHz, CD_2Cl_2) δ: 7.38–7.35 (d, 4H, arom), 7.32–7.29 (d, 2H, arom), 7.10–7.08 (d, 2H, arom), 7.01–6.98 (d, 4H, arom), 4.64 (s, 2H, arom), 3.10 (s, 2H, CH), 1.95 (br s, 1H, OH) ^{13}C NMR (75 MHz, CD_2Cl_2) δ: 148.2, 146.4, 138.0, 133.7, 128.9, 126.2, 123.7, 116.4, 84.1, 77.1, 65.4
7	^{1}H NMR (300 MHz, DMSO-d_6) δ: 8.56–8.54 (m, 4H, arom), 7.85–7.76 (m, 6H, arom), 7.38–7.28 (m, 6H, arom), 7.07–7.04 (m, 6H, arom), 5.75 (s, 4H, CH_2), 5.15 (t, 1H, OH), 4.48–4.49 (d, 2H, CH_2OH) ^{13}C NMR (75 MHz, DMSO-d_6) δ: 154.9, 149.2, 146.6, 146.2, 145.2, 137.8, 137.2, 127.8, 126.2, 124.9, 124.3, 123.2, 123.1, 121.9, 121.4, 62.4, 54.4

Table 2. Elemental analysis and yield of the newly prepared compounds **4**, **6**, and **7**

Compound	Formula	M_W	w_i (calc.)/mass % w_i (found)/mass %			Yield
		g mol^{-1}	C	H	N	%
4	$C_{19}H_{15}I_2NO$	527.1	43.29	2.87	2.66	98
			43.37	2.68	2.75	
6	$C_{23}H_{17}NO$	323.4	85.42	5.30	4.33	98
			85.60	5.21	4.30	
7	$C_{35}H_{29}N_9O$	591.7	71.05	4.94	21.31	97
			71.24	4.85	21.17	

titania composites and the BET specific surface area of bare supports. The obtained values were very similar for the two organic–inorganic materials, 0.14 molecules per nm^2 for DS-Anatase and 0.16 molecules per nm^2 for DS-P25.

XRPD was used to identify crystallographic phases of the synthesized titania nanocrystals and the two final hybrid materials (Fig. 3). Diffraction pattern of the synthesized TiO_2, after the calcination at 550℃, exhibited well-resolved reflections at 2θ values of 25.44℃, 38.02°, 48.19°, 53.94°, 54.98°, and 63.06°, corresponding to the characteristic pattern of anatase (the only present crystalline phase of TiO_2, JCPDS 84-1286).

Mass-average size of the titania crystallites in the synthesized TiO_2 sample was calculated by the Fourier analysis of the (101) diffraction line and found to be 15 nm, i.e. smaller than the value indicated by TEM. This can be attributed to the observed presence of multi-grained particles and the inner porous structure of the particles. XRPD profiles are in fact related to the size of the coherent scattering areas, not to the size of the particles. For this reason, the two techniques give similar values only in case of perfectly ordered single-crystal particles; in all other cases, XRPD gives lower values than microscopy. For Degussa P25, a value of 19 nm was found, which is higher than that obtained for the anatase sample but lower than its nominal value.

Since titania surface is characterized by the presence of various types of hydroxyl groups, which differ according to the type and number of Ti atoms to which they are bonded, infrared spectroscopy is an important tool to differentiate these groups and understand their interaction with organic molecules (Finnie et al., 2001; Lobo-Lapidus & Gates, 2010; Zhang et al., 2006). The surface hydroxyls can be either free (isolated Ti—OH), hydrogen bonded one to another (vicinal) or bonded to water molecules chemically adsorbed on the TiO_2 surface.

Infrared spectra of the mesoporous anatase and Degussa P25 supports and the respective two hybrid organic–inorganic materials are shown in Fig. 4. In all DRIFT-IR spectra of the titania samples, a broad absorption band in the region of 3800–2800 cm^{-1} dominates. This broad band, centered at 3300 cm^{-1}, is attributed to the OH-stretching vibrations of free and hydrogen-bonded surface hydroxyl groups of titania. A small peak due to the Ti—OH hydroxyl modes at 3693 cm^{-1} is present in the profile of both titania sup-

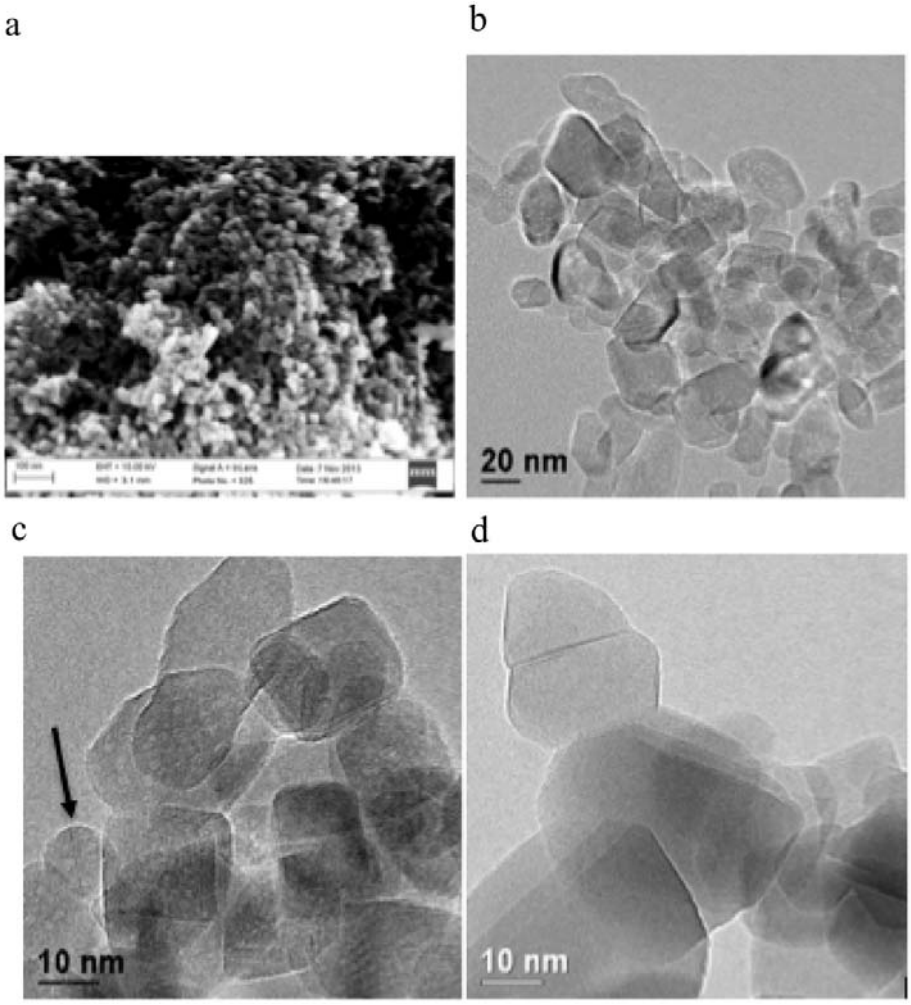

Fig. 2. Micrographs: large-scale SEM image (a), TEM (b), and HRTEM (c) images of the fresh synthesized anatase titania (arrow shows a particle with a twin crystal structure); HRTEM (d) image of the Degussa P25 sample.

ports. The wide peak at around 800 cm^{-1} to 500 cm^{-1} is the sum of the two stretching mode vibrations assigned to the Ti—O and O—Ti—O vibrations of titania.

Grafting of the dye to the supports was accompanied by changes in the Ti—OH stretching modes (Fig. 4). A decrease of the intensity of the peak due to the Ti—OH hydroxyl modes with a slight shift to lower frequencies (from 3693 cm^{-1} to 3687 cm^{-1}) was registered in both the DS-Anatase and DS-P25 composites, most probably due to the interaction of the benzyl alcohol functionality of the organic molecule with the surface of titania. These data suggest the attachment of the dye on the surface through an interaction of titania hydroxyls with the OH groups of DS. No modifications of the vibrational modes of pyridyl moieties were detected in the IR spectra, most probably due to the small amount of organic molecules. In any case, interaction of titania with pyridyl moieties and extended π systems of the triazole rings cannot be excluded. Infrared spectra of the composites show the presence of two bands at 1587 cm^{-1} and

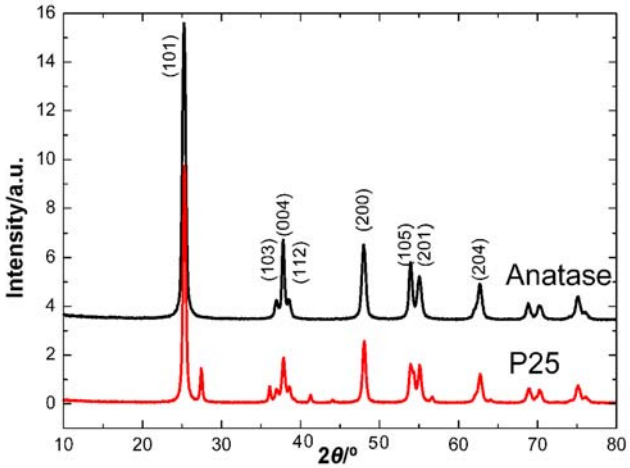

Fig. 3. X-Ray diffraction patterns of the two titania supports. The Miller indexes belong to the anatase phase; the extra peaks in the P25 sample show the presence of a second component of TiO_2, the rutile phase.

1492 cm^{-1} attributable to the C—C stretching mode of the benzenoid (B) rings. The bands at 1290 cm^{-1}

Table 3. Binding energies and C/N atomic ratio of the dye and the two hybrid materials calculated by XPS

Sample	C 1s/eV	O 1s/eV	N 1s/eV	C/N atomic ratio
DS	284.8 (80 %) 286.0 (18 %) 292.1 (2 %)	532.9 (91 %) 533.8 (9 %)	399.2 (74 %) 401.2 (26 %)	5.56
DS-P25	284.8 (83 %) 286.1 (12 %) 288.7 (5 %)	529.9 (87 %) 531.6 (13 %)	399.6 (79 %) 401.3 (21 %)	13.21
DS-Anatase	284.8 (80 %) 286.1 (14 %) 288.6 (6 %)	529.9 (90 %) 531.7 (10 %)	399.7 (82 %) 401.1 (28 %)	15.39

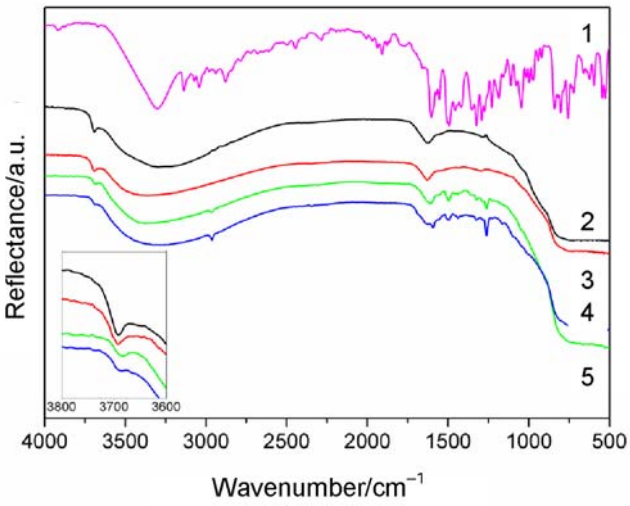

Fig. 4. Infrared spectra of the dye sensitizer (1), bare titania supports P25 (2) and anatase (3), and the two hybrid organic–inorganic materials DS-P25 (4) and DS-Anatase (5). In the inset: magnification of the region of 3800–3600 cm^{-1}.

and 1226 cm^{-1} can be attributed to the C—N stretching mode of the benzenoid unit confirming the presence of DS on the support.

Surface of the DS-Anatase composite was investigated by X-ray photoelectron spectroscopy. The N 1s spectrum shows two contributions at 399.3 eV (74 %) and 401.2 eV (26 %). The first one was assigned to the pyrrolidinic and triazolic moieties; and the second one to protonated nitrogen (Lázaro Martínez et al., 2011).

Table 3 shows the XPS binding energy values and the proportions of the different contributions in some signals such as C 1s, N 1s, and O 1s.

In our system, nitrogen is the representative atom of the chromophore because the supports do not contain nitrogen-containing compounds. The N 1s signal of the DS chromophore forming part of the composite materials does not show any significant changes in the shape and binding energy values; however, a slightly lower protonation degree was observed. This means that the interactions between the chromophore and the support are weak.

The C 1s core level spectrum of the dye sensitizer (Fig. 5a) can be decomposed into three contributions: at 284.8 eV (80 %), 286.0 eV (18 %), and at 292.1 eV (2 %). The last contribution, at 292.1 eV, with a very low intensity of the C 1s signal, is due to the presence of π–π^* interactions. After the adsorption on anatase, the C 1s signal exhibited a lower intensity in comparison with the C 1s signal of DS (Fig. 5b); the shape of the spectra is more or less similar with three contributions at 284.8 eV (80 %), 286.1 eV (14 %), and 288.6 eV (6 %). The contribution at high binding energy is also shown in the C 1s spectrum of anatase probably due to the presence of surface carbonate.

All Ti 2p spectra are very similar, with the Ti $2p_{3/2}$ binding energy values of 458.4–458.7 eV, typical of titania.

The surface C/N atomic ratio measured by XPS for the DS powder is 5.56. This value is higher than both the theoretical value (3.88) and the value found by elemental analysis (4.02), which suggests the presence of some adventitious carbon on the powder surface. For both hybrid materials, DS-P25 and DS-Anatase, experimental values of the surface C/N atomic ratio obtained by XPS are even higher (13.21 and 15.30, respectively) and much higher than the values found by elemental analysis (5.88 and 5.73, respectively). The high C/N atomic ratios observed on the surface of the hybrid material can be partly due to the presence of more adventitious carbons since, in this case, the amount of this contaminant is likely to be more relevant. However, the large increase in the C/N ratio observed by XPS suggests the presence of the dye at the surface of the supports.

Optical properties of the DS dye were fully investigated and the results well match with those observed for analogous dyes in previous reports (Lázaro Martínez et al., 2011; Ning et al., 2008; Ning & Tian, 2009; Cai et al., 2013; Zhang et al., 2009b, 2012).

In Fig. 6, absorption, emission (PL, $\lambda_{ex} = 370$ nm), and excitation (PLE, $\lambda_{em} = 550$ nm) spectra recorded

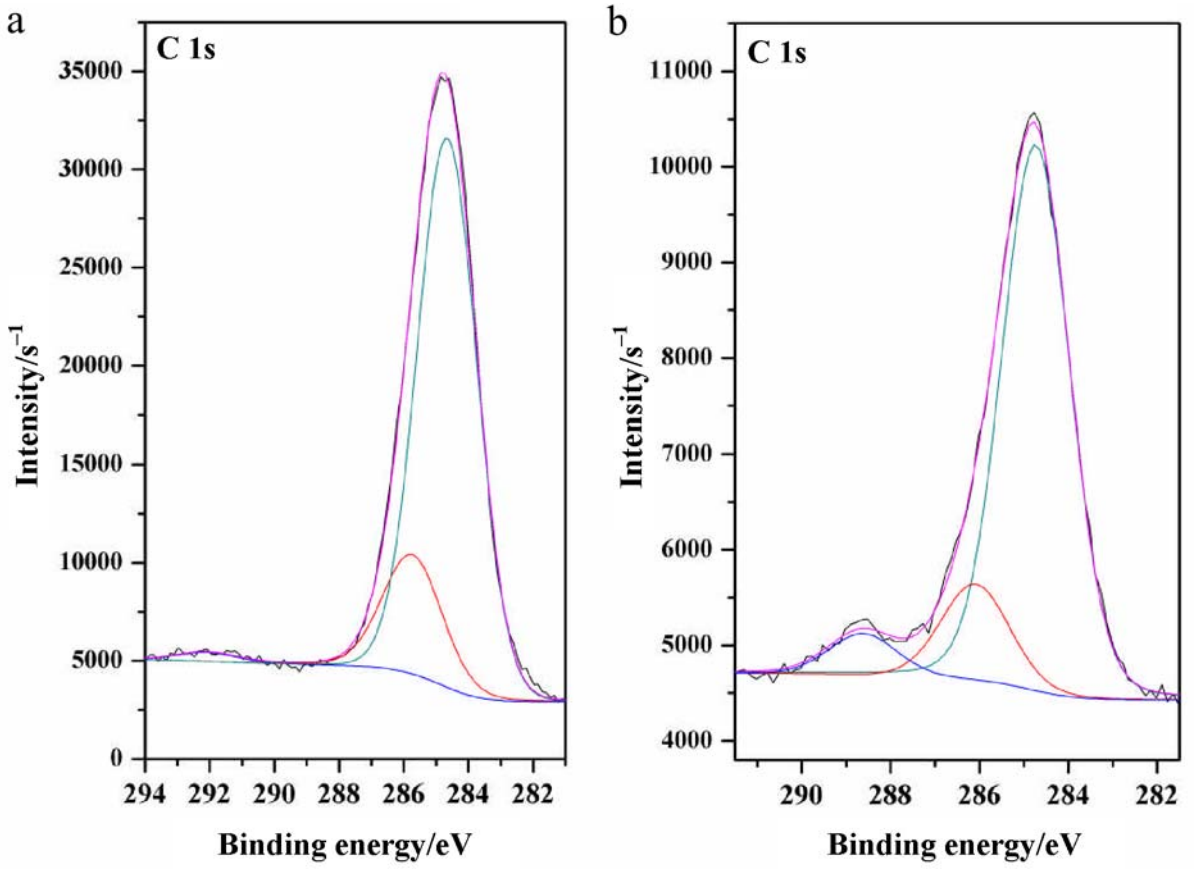

Fig. 5. C 1s core level spectra of the samples: DS chromophore (a) and DS-Anatase composite (b).

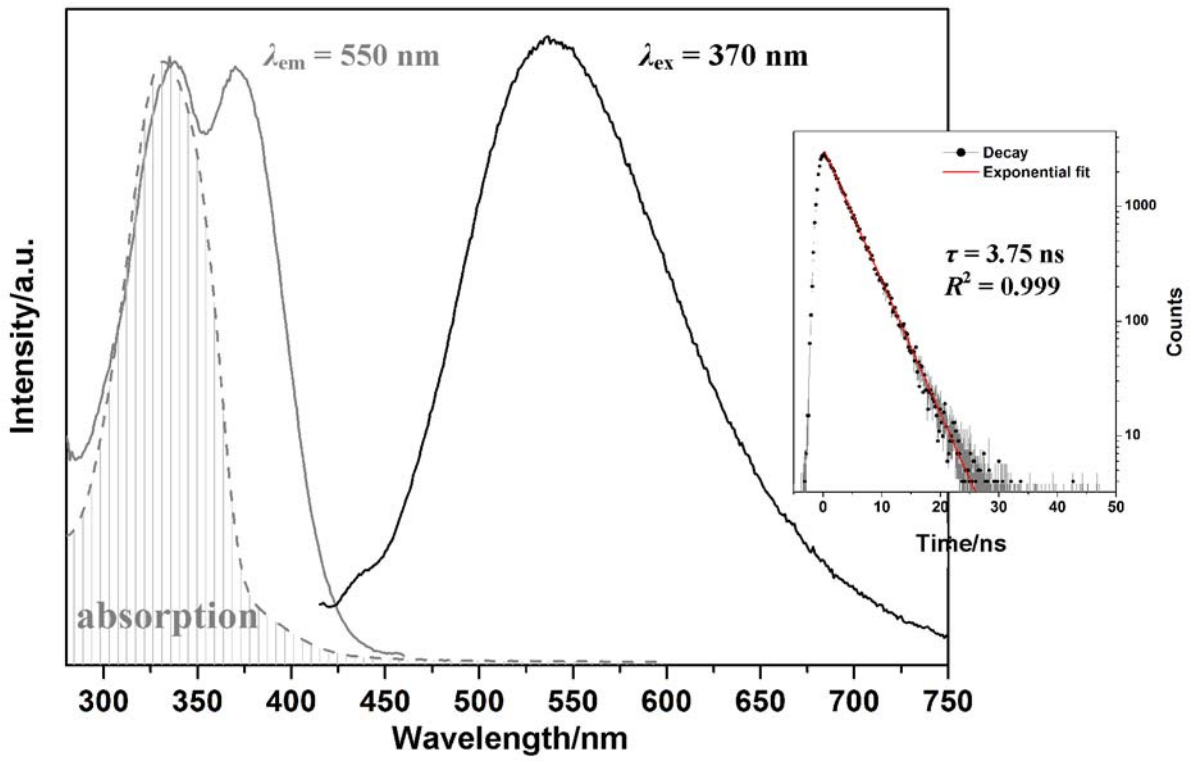

Fig. 6. Absorption, excitation, and emission spectra of the dye recorded in chloroform at the concentration of 10^{-5} M. In the inset: decay curve and exponential fit.

in chloroform are shown.

The molecule has an extinction coefficient of 7.4×10^4 cm^{-1} M^{-1} at the maximum of the absorption band (peaked at 331 nm), which is a value similar to those reported in other papers for similar molecules (Ning & Tian, 2009; Cai et al., 2013). A smaller shoulder can be observed at longer wavelengths. This transition is much more evident in the PLE spectrum which shows two bands with comparable intensity peaked at 335 nm and 373 nm respectively. For triarylamines, the absorptions in the 300–400 nm range originate in from the π–π^* transitions (Ning et al., 2008; Ning & Tian, 2009; Cai et al., 2013). The band above 400 nm observed in other triarylamine molecules was not observed here because of the absence of a good electron acceptor group, such as the cyanoacrylic acid moiety enabling intramolecular charge transfer (ICT). The DS behavior here resembles that of the dye synthesized by Zhang et al. (2009b). Although the molecules differ significantly, an electron acceptor group is absent in both of them and they display a quite similar absorption spectrum with almost null extinction coefficient above 400 nm.

The emission spectrum shows a rather broad emission peak centered at 530 nm extending up above 750 nm which results in a yellow–greenish fluorescence. The PL and PLE spectra display a rather large Stokes-shift of more than 150 nm.

The PL decay curve, recorded exciting DS at 373 nm and monitoring the emission at 550 nm, can be fitted using a single exponential with the time constant: $\tau = 3.75$ ns, in accordance with the values reported in literature for similar compounds (Zhang et al., 2012).

Due to the great attention drawn by the triarylamine family of molecules for DSSC applications, the study of the optical behavior of the hybrid DS-TiO_2 composite is of great interest in this application field. In particular, by impregnating the chromophore on titania, it is possible to extend the harvesting capability of the cell with respect to bare titanium dioxide.

In Fig. 7, absorption spectra of the DS-TiO_2 hybrid composites, obtained either using the freshly synthesized pure phase anatase TiO_2 or the commercial P25 Degussa, are shown.

A bathochromic shift of the DS absorption when adsorbed on an inorganic support with respect to the diluted monomeric form was observed, which is usually ascribed to the occurrence of *J*-aggregation (supramolecular self-organization) (He et al., 2011). It should be noted that, in spite of the very similar dye loading, the behavior of the two DS-TiO_2 composites is slightly different, with the dye showing a stronger absorption capability when adsorbed onto synthesized anatase. This is also confirmed by the different color of the two obtained solids. As mentioned in the Experimental part, the DS-Anatase sample is more yellowish than the DS-P25 one which is rather

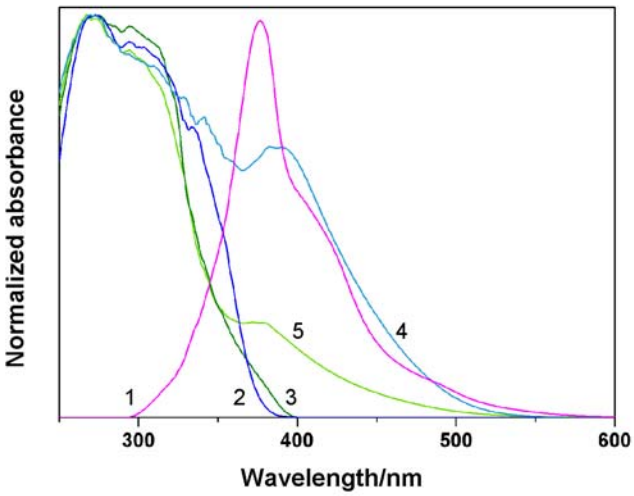

Fig. 7. Absorption spectra of the dye sensitizer (1), bare synthesized anatase (2) and commercial P25 (3) titania, and the respective composites DS-Anatase (4) and DS-P25 (5).

grayish. The cause of this difference in the absorption features of the composites suggests a different interaction with the two surfaces. In fact, the role of the different crystalline forms of titania and the different photoactivity of the different exposed external surfaces were thoroughly investigated, especially in regard to the influence on the photocatalytic properties (D'Arienzo et al., 2011; Scotti et al., 2009; Testino et al., 2007). For DSSCs, a more efficient role of anatase nanocrystals had already been suggested by Barbé et al. (1997), whereas the lower electron-hole recombination rate of geometrically anisotropic nanoparticles has been demonstrated more recently (D'Arienzo et al. (2011) and references therein).

In the present case, the presence of the pores in the nanoparticles of the anatase sample can also play a role hosting some molecules and potentially shielding them from the outer environment. Furthermore, P25 is composed of a mixture of anatase : rutile (approximately 20 : 80), which causes different optical behavior with respect to pure anatase. An analysis of the absorption features of the synthesized pure phase anatase gives a band gap of 3.24 eV, in fairly good agreement with the reported band-gap of anatase (3.2 eV). Rutile is known to possess a band-gap of 3.0 eV (Reyes-Coronado et al., 2008), thus, Degussa P25 is expected to display a smaller gap as it is the case; the band gap of the mixture can be estimated as predominantly lying in the range of 3.0–3.1 eV. Also, this difference in the optical properties is expected to play a role in the different behavior of the composites.

Conclusions

An efficient synthetic strategy based on a "click" reaction allowing obtaining the prototype of a new

class of chromophores with a hydroxyl anchoring group has been devised. Taking advantage of the "click" character of the [3+2] azide–alkyne coupling, it was possible to obtain the desired chromophore with an overall yield as high as 70 %. Our investigations suggest that the benzylic alcohol functionality present at the focal point of the branched structure of the chromophore is able to interact with the OH groups of the TiO_2; very interestingly, the nature of TiO_2 seems to play a significant specific role in the determination of the optical activity of the resulting hybrid materials.

Further investigations are in progress aiming to test the optical activity of the DS-Anatase composite on a DSSC device, since its enhanced light harvesting properties make it a promising material for such applications. In fact, the developed branched triphenylamine-based structure is expected to improve the device performance by reducing intermolecular interactions and minimizing dye aggregation.

Further improvements could also be easily implemented by application of the chelating triazole-pyridyl system to host suitable transition metal fragments (e.g., ruthenium).

Acknowledgements. The authors acknowledge financial support from the Universities of Venice and Málaga and the Consortium INSTM (Italy). Projects CTQ2012-37925-C03-03 and CTQ2012-30703 of Ministerio de Economía y Competitividad (Spain) and project of Excellence P12 RNM 1565 (Junta de Andalucía, Spain) are also acknowledged for financial support.

References

Amadio, E., Bertoldini, M., Scrivanti, A., Chessa, G., Beghetto, V., Matteoli, U., Bertani, R., & Dolmella, A. (2011). Synthesis, crystal structure, solution behaviour and catalytic activity of a palladium(II)-allyl complex containing a 2-pyridyl-1,2,3-triazole bidentate ligand. *Inorganica Chimica Acta*, *370*, 388–393. DOI: 10.1016/j.ica.2011.02.002.

Ardo, S., & Meyer, G. J. (2009). Photodriven heterogeneous charge transfer with transition-metal compounds anchored to TiO_2 semiconductor surfaces. *Chemical Society Reviews*, *38*, 115–164. DOI: 10.1039/b804321n.

Armarego, W. L. F., & Perrin, D. D. (1996). *Purification of laboratory chemicals* (4th ed.). Oxford, UK: Butterworth-Heinemann.

D'Arienzo, M., Carbajo, J., Bahamonde, A., Crippa, M., Polizzi, S., Scotti, R., Wahba, L., & Morazzoni, F. (2011). Photogenerated defects in shape-controlled TiO_2 anatase nanocrystals: A probe to evaluate the role of crystal facets in photocatalytic processes. *Journal of the American Chemical Society*, *133*, 17652–17661. DOI: 10.1021/ja204838s.

Barbé, C. J., Arendse, F., Comte, P., Jirousek, M., Lenzmann, F., Shklover, V., & Grätzel, M. (1997). Nanocrystalline titanium oxide electrodes for photovoltaic applications. *Journal of the American Ceramic Society*, *80*, 3157–3171. DOI: 10.1111/j.1151-2916.1997.tb03245.x.

Barnard, A. S., & Curtiss, L. A. (2005). Prediction of TiO_2 nanoparticle phase and shape transitions controlled by surface chemistry. *Nano Letters*, *5*, 1261–1266. DOI: 10.1021/nl050355m.

Bolje, A., Urankar, D., & Košmrlj, J. (2014). Synthesis and NMR analysis of 1,4-disubstituted 1,2,3-triazoles tethered to pyridine, pyrimidine, and pyrazine rings. *European Journal of Organic Chemistry*, *36*, 8167–8181. DOI: 10.1002/ejoc.201403100.

Brotherton, W. S., Michaels, H. A., Simmons, J. T., Clark, R. J., Dalal, N. S., & Zhu, L. (2009). Apparent copper(II)-accelerated azide-alkyne cycloaddition. *Organic Letters*, *11*, 4954–4957. DOI: 10.1021/ol9021113.

Cai, S. Y., Hu, X. H., Zhang, Z. Y., Su, J. H., Li, X., Islam, A., Han, L. Y., & Tian, H. (2013). Rigid triarylamine-based efficient DSSC sensitizers with high molar extinction coefficients. *Journal of Materials Chemistry A*, *1*, 4763–4772. DOI: 10.1039/c3ta01657a.

Chen, D. H., Huang, F. Z., Cheng, Y. B., & Caruso, R. A. (2009). Mesoporous anatase TiO_2 beads with high surface areas and controllable pore sizes: A superior candidate for high-performance dye-sensitized solar cells. *Advanced Materials*, *21*, 2206–2210. DOI: 10.1002/adma.200802603.

De Jesus Trindade, F., Queiruga Rey, J. F., & Brochsztain, S. (2011). Covalent attachment of 4-amino-1,8-naphthalimides onto the walls of mesoporous molecular sieves MCM-41 and SBA-15. *Dyes and Pigments*, *89*, 97–104. DOI: 10.1016/j.dyepig.2010.09.009.

Duan, T. N., Fan, K., Fu, Y., Zhong, C., Chen, X. G., Peng, T. Y., & Qin, J. G. (2012). Triphenylamine-based organic dyes containing a 1,2,3-triazole bridge for dye-sensitized solar cells via a 'click' reaction. *Dyes and Pigments*, *94*, 28–33. DOI: 10.1016/j.dyepig.2011.11.008.

Enzo, S., Polizzi, S., & Benedetti, A. (1985). Application of fitting techniques to the Warren-Averbach method for X-ray line broadening analysis. *Zeitschrift für Kristallographie*, *170*, 275–287. DOI: 10.1524/zkri.1985.170.14.275.

Enzo, S., Fagherazzi, G., Benedetti, A., & Polizzi, S. (1988). A profile-fitting procedure for analysis of broadened X-ray diffraction peaks. I. Methodology. *Journal of Applied Crystallography*, *21*, 536–542. DOI: 10.1107/s0021889888006612.

Finnie, K. S., Cassidy, D. J., Bartlett, J. R., & Woolfrey, J. L. (2001). IR spectroscopy of surface water and hydroxyl species on nanocrystalline TiO_2 films. *Langmuir*, *17*, 816–820. DOI: 10.1021/la0009240.

Ganschow, M., Wark, M., Wöhrle, D., & Schulz-Ekloff, G. (2000). Anchoring of functional dye molecules in MCM-41 by microwave-assisted hydrothermal cocondensation. *Angewandte Chemie International Edition*, *39*, 160–163. DOI: 10.1002/(SICI)1521-3773(20000103)39:1<160::AID-ANIE160>3.0.CO;2-V.

Gómez-Romero, P., & Sanchez, C. (Eds.) (2004). *Functional hybrid materials*. Weinheim, Germany: Wiley-VCH.

Grätzel, M. (2009). Recent advances in sensitized mesoscopic solar cells. *Accounts of Chemical Research*, *42*, 1788–1798. DOI: 10.1021/ar900141y.

Gu, X., Zhou, L., Li, Y. W., Sun, Q. A., & Jena, P. (2012). Design of new metal-free dyes for dye-sensitized solar cells: A first-principles study. *Physics Letters A*, *376*, 2595–2599. DOI: 10.1016/j.physleta.2012.07.020.

Hagberg, D. P., Yum, J. H., Lee, H. J., De Angelis, F., Marinado, T., Karlson, K. M., Humphry-Baker, R., Sun, L. C., Hagfeldt, A., Grätzel, M., & Nazeeruddin, M. K. (2008). Molecular engineering of organic sensitizers for dye-sensitized solar cell applications. *Journal of the American Chemical Society*, *130*, 6259–6266. DOI: 10.1021/ja800066y.

Hagfeldt, A., Boschloo, G., Sun, L. C., Kloo, L., & Pettersson, H. (2010). Dye-sensitized solar cells. *Chemical Reviews*, *110*, 6595–6663. DOI: 10.1021/cr900356p.

Harima, Y., Fujita, T., Kano, Y., Imae, I., Komaguchi, K., Ooyama, Y., & Ohshita, J. (2013). Lewis-acid sites of TiO_2 surface for adsorption of organic dye having pyridyl group as

anchoring unit. *The Journal of Physical Chemistry C*, *117*, 16364–16370. DOI: 10.1021/jp405835y.

He, J. X., Wu, W. J., Hua, J. L., Jiang, Y. H., Qu, S. Y., Li, J., Long, Y. T., & Tian, H. (2011). Bithiazole-bridged dyes for dye-sensitized solar cells with high open circuit voltage performance. *Journal of Materials Chemistry*, *21*, 6054–6062. DOI: 10.1039/c0jm03811c.

Katono, M., Bessho, T., Meng, S., Humphry-Baker, R., Rothenberger, G., Zakeeruddin, S. M., Kaxiras, E., & Grätzel, M. (2011). D-π-A dye system containing cyano-benzoic acid as anchoring group for dye-sensitized solar cells. *Langmuir*, *27*, 14248–14252. DOI: 10.1021/la203104v.

Kolb, H. C., Finn, M. G., & Sharpless, K. B. (2001). Click chemistry: Diverse chemical function from a few good reactions. *Angewandte Chemie International Edition, 40,* 2004–2021. DOI: 10.1002/1521-3773(20010601)40:11<2004::AID-ANIE2004>3.0.CO;2-5.

Latterini, L., Nocchetti M., Aloisi, G. G., Costantino, U., & Elisei, F. (2007). Organized chromophores in layered inorganic matrices. *Inorganica Chimica Acta*, *360*, 728–740. DOI: 10.1016/j.ica.2006.07.048.

Lázaro Martínez, J. M., Rodríguez-Castellón, E., Torres Sánchez, R. M., Denaday, L. R., Buldain, G. Y., & Campo Dall'Orto, V. (2011). XPS studies on the Cu(I,II)–polyampholyte heterogeneous catalyst: An insight into its structure and mechanism. *Journal of Molecular Catalysis A: Chemical, 339,* 43–51. DOI: 10.1016/j.molcata.2011.02.010.

Li, Z. A., Wu, W. B., Li, Q. Q., Yu, G., Xiao, L., Liu, Y. Q., Ye, C., Qin, J., & Li, Z. (2010). High-generation second-order nonlinear optical (NLO) dendrimers: Convenient synthesis by click chemistry and the increasing trend of NLO effects. *Angewandte Chemie International Edition*, *49*, 2763–2767. DOI: 10.1002/anie.200906946.

Lobo-Lapidus, R. J., & Gates, B. C. (2010). Probing surface sites of TiO_2: Reactions with $[HRe(CO)_5]$ and $[CH_3Re(CO)_5]$. *Chemistry – A European Journal*, *16*, 11386–11398. DOI: 10.1002/chem.201000267.

Mao, J. Y., He, N. N., Ning, Z. J., Zhang, Q., Guo, F. L., Chen, L., Wu, W. J., Hua, J. L., & Tian, H. (2012). Stable dyes containing double acceptors without COOH as anchors for highly efficient dye-sensitized solar cells. *Angewandte Chemie International Edition*, *51*, 9873–9876. DOI: 10.1002/anie.201204948.

Michinobu, T., Satoh, N., Cai, J. H., Li, Y. R., & Han, L. Y. (2014). Novel design of organic donor–acceptor dyes without carboxylic acid anchoring groups for dye-sensitized solar cells. *Journal of Materials Chemistry C*, *2*, 3367–3372. DOI: 10.1039/c3tc32165g.

Moretti, E., Storaro, L., Chessa, G., Talon, A., Callone, E., Mueller, K. J., Enrichi, F., & Lenarda, M. (2012). Stepwise dansyl grafting on the kaolinite interlayer surface. *Journal of Colloid and Interface Science*, *375*, 112–117. DOI: 10.1016/j.jcis.2012.02.033.

Nazeeruddin, M. K., Humphry-Baker, R., Officer, D. L., Campbell, W. M., Burrell, A. K., & Grätzel, M. (2004). Application of metalloporphyrins in nanocrystalline dye-sensitized solar cells for conversion of sunlight into electricity. *Langmuir*, *20*, 6514–6517. DOI: 10.1021/la0496082.

Ning, Z., Chen, Z., Zhang, Q., Yan, Y., Qian, S., Cao, Y., & Tian, H. (2007). Aggregation-induced emission (AIE)-active starburst triarylamine fluorophores as potential non-doped red emitters for organic light-emitting diodes and Cl_2 gas chemodosimeter. *Advanced Functional Materials*, *17*, 3799–3807. DOI: 10.1002/adfm.200700649.

Ning, Z. J., Zhang, Q., Wu, W. J., Pei, H. C., Liu, B., & Tian, H. (2008). Starburst triarylamine based dyes for efficient dye-sensitized solar cells. *The Journal of Organic Chemistry*, *73*, 3791–3797. DOI: 10.1021/jo800159t.

Ning, Z. J., & Tian, H. (2009). Triarylamine: a promising core unit for efficient photovoltaic materials. *Chemical Communications*, *2009*, 5483–5495. DOI: 10.1039/b908802d.

Ooyama, Y., Nagano, T., Inoue, S., Imae, I., Komaguchi, K., Ohshita, J., & Harima, Y. (2011). Dye-sensitized solar cells based on donor-π-acceptor fluorescent dyes with a pyridine ring as an electron-withdrawing-injecting anchoring group. *Chemistry – A European Journal*, *17*, 14837–14843. DOI: 10.1002/chem.201101923.

Parent, M., Mongin, O., Kamada, K., Katan, C., & Blanchard-Desce, M. (2005). New chromophores from click chemistry for two-photon absorption and tuneable photoluminescence. *Chemical Communications*, *2005*, 2029–2031. DOI: 10.1039/b419491h.

Park, S. H., Ogino, K., & Sato, H. (2000). Synthesis and characterization of photorefractive polymers with triphenylamine unit and NLO chromophore unit on a side chain. *Polymers for Advanced Technologies*, *11*, 349–358. DOI: 10.1002/1099-1581(200007)11:7<349::AID-PAT978>3.0.CO;2-Z.

Pesek, J. J. (1990). Some new perspectives on the chemical modification of silica. In D. E. Leyden, & W. T. Collins (Eds.), *Chemically modified oxide surfaces* (Vol. *3*, pp. 93–107*)*. New York, NY, USA: Gordon & Breach.

Rostovtsev, V. V., Green, L. G., Fokin, V. V., & Sharpless, K. B. (2002). A stepwise Huisgen cycloaddition process: Copper(I)-catalyzed regioselective "ligation" of azides and terminal alkynes. *Angewandte Chemie International Edition*, *41*, 2596–2599. DOI: 10.1002/1521-3773(20020715)41:14<2596::AID-ANIE2596>3.0.CO;2-4.

Reyes-Coronado, D., Rodríguez-Gattorno, G., Espinosa-Pesqueira, M. E., Cab, C., de Coss, R., & Oskam, G. (2008). Phase-pure TiO_2 nanoparticles: anatase, brookite and rutile. *Nanotechnology*, *19*, 145605. DOI: 10.1088/0957-4484/19/14/145605.

Scotti, R., D'Arienzo, M., Testino, A., & Morazzoni, F. (2009). Photocatalytic mineralization of phenol catalyzed by pure and mixed phase hydrothermal titanium dioxide. *Applied Catalysis B: Environmental*, *88*, 497–504. DOI: 10.1016/j.apcatb.2008.10.017.

Segal-Peretz, T., Jahnke, J. P., Berenson, A., Neeman, L., Oron, D., Rossini, A. J., Chmelka, B. F., & Frey, G. L. (2014). Understanding and promoting molecular interactions and charge transfer in dye-mediated hybrid photovoltaic materials. *The Journal of Physical Chemistry C*, *118*, 25374–2539. DOI: 10.1021/jp508819w.

Sharifi, N., Tajabadi, F., & Taghavinia, N. (2014). Recent developments in dye-sensitized solar cells. *ChemPhysChem*, *15*, 3902–3927. DOI: 10.1002/cphc.201402299.

Testino, A., Bellobono, I. R., Buscaglia, V., Canevali, C., D'Arienzo, M., Polizzi, S., Scotti, R., & Morazzoni, F. (2007). Optimizing the photocatalytic properties of hydrothermal TiO_2 by the control of phase composition and particle morphology. A systematic approach. *Journal of the American Chemical Society*, *129*, 3564–3575. DOI: 10.1021/ja067050+.

Urankar, D., Pinter, B., Pevec, A., De Proft, F., Turel, I., & Košmrlj, J. (2010). Click-triazole N2 coordination to transition-metal ions is assisted by a pendant pyridine substituent. *Inorganic Chemistry*, *49*, 4820–4829. DOI: 10.1021/ic902354e.

Wang, Z. S., Huang, Y. Y., Cheng, C. H., Zheng, J., Cheng, H. M., & Tian, S. J. (2000). Photosensitization of ITO and nanocrystalline TiO_2 electrode with a hemicyanine derivative. *Synthetic Metals*, *114*, 201–207. DOI: 10.1016/s0379-6779(00)00261-7.

Zhang, L. X., Liu, P., & Su, Z. X. (2006). Preparation of PANI–TiO_2 nanocomposites and their solid-phase photocatalytic degradation. *Polymer Degradation and Stability*, *91*, 2213–2219. DOI: 10.1016/j.polymdegradstab.2006.01.002.

Zhang, G. L., Bala, H. R., Cheng, Y. M., Shi, D., Lv, X. J., Yu, Q. J., & Wang, P. (2009a). High efficiency and stable dye sensitized solar cells with an organic chromophore featuring a binary π-conjugated spacer. *Chemical Communications*, *2009*, 2198–2200. DOI: 10.1039/b822325d.

Zhang, Q., Ning, Z. J., & Tian, H. (2009b). 'Click' synthesis of starburst triphenylamine as potential emitting material. *Dyes and Pigments*, *81*, 80–84. DOI: 10.1016/j.dyepig.2008.09.005.

Zhang, M. D., Pan, H., Ju, X. H., Ji, Y. J., Qin, L., Zheng, H. G., & Zhou, X. F. (2012). Improvement of dye-sensitized solar cells' performance through introducing suitable heterocyclic groups to triarylamine dyes. *Physical Chemistry Chemical Physics*, *14*, 2809–2815. DOI: 10.1039/c2cp23876d.

Zhao, W. J., Li, D. M., He, B., Zhang, J. L., Huang, J. Z., & Zhang, L. Z. (2005). The photoluminescence of coumarin derivative encapsulated in MCM-41 and Ti-MCM-41. *Dyes and Pigments*, *64*, 265–270. DOI: 10.1016/j.dyepig.2004.06.002.